Longitudinal-strain soliton focusing in a narrowing nonlinearly elastic rod

A. M. Samsonov, G. V. Dreiden, A. V. Porubov, and I. V. Semenova
A. F. Ioffe Physical Technical Institute of the Russian Academy of Sciences, St. Petersburg 194021, Russia
(Received 23 June 1997; revised manuscript received 23 October 1997)

The evolution of a longitudinal-strain solitary wave (a soliton) is studied theoretically and in experiments in a nonlinearly elastic tapered rod. Amplification (focusing) of the soliton is predicted and observed in the rod with decreasing cross section. An asymmetric soliton deformation when focused is observed. An approach is developed to obtain analytical relationships between longitudinal and shear nonlinear strains, and an asymptotic solution to the problem is found, accurately satisfying the boundary conditions on the lateral rod's surface. The explicit relationship is obtained for the soliton amplitude dependence upon the cross section radius' variations of the nonlinearly elastic rod. An allowed interval of soliton velocities is shown to exist that is dependent on elasticity. It was proved in experiments that the elastic strain soliton is not absorbed even at distances much greater than the typical linear dissipation length for linear waves in polystyrene. [S0163-1829(98)10309-0]

I. INTRODUCTION

This paper is devoted to the theoretical and experimental description of the propagation and amplification of the strain solitary wave (soliton) in a cylindrical nonlinearly elastic rod with varying cross section. We call it an inhomogeneous rod in the following for convenience, while the rod with a permanent cross section will be called the homogeneous one.

Solitons in fluids were observed and generated many times; see, e.g., Refs. 1 and 2. It was the most surprising fact, however, that despite an almost similar description of stresses in fluids and solids (see, e.g., some fundamental books[3–5]) longitudinal-strain solitons have not been observed in nonlinearly elastic waveguides. Envelope solitary waves governed by the nonlinear Schrödinger equation were widely considered; another famous soliton in a solid, being modeled as a ball chain, was found by Frenkel and Kontorova in 1938 and became useful for crystalline lattice models. However, there must be a soliton in solids in the form of a nonlinear *long* quasistationary localized strain wave, propagating either along an interface (internal solitary wave) or inside a waveguide (a density soliton).

The soliton propagates without change of shape in a uniform rod while its shape will vary in the presence of inhomogeneities. In the last case amplification or focusing may occur; in other words, the soliton amplitude will increase, while its width will decrease simultaneously. Then the localized area of plasticity and even fracture of a waveguide may happen to appear, which can be of practical importance.

The complete description of a three-dimensional (3D) nonlinear wave in a continuum is a difficult problem, which is why initial 3D problems are usually reduced to the 1D form in order to clarify the simplest but qualitatively new *analytical* solutions. Very often the linearization of a problem was done; however, it turns out to be unsatisfactory from the genuine physical point of view, because the ratio of a finite deformation and its linear part is determined by a displacement gradient and its variation in time; see, e.g., Refs. 5–9.

Dealing with nonlinear elasticity, one can reduce the dimension of the problem using the waveguide geometry, the wave solution class, and an appropriate type of nonlinearly elastic material. In particular, the simplest ''single-mode'' model[7] for a cylindrical elastic isotropic rod is based on the following physical *assumptions* about displacements and strains inside the rod: The curvature of a cross section after deformation is negligible, and the Poisson effect is taken into account. Then the so-called plane cross section hypothesis is assumed to be valid for the displacements along the rod axis x, $u(x,r,t)=U(x,t)$, while the shear displacements $w(x,r,t)$ are determined by longitudinal strains by means of the Love relationship $w=-\nu r U_x$.[10] Here r is the radial coordinate, t is time, and ν is the Poisson coefficient. This model has been used recently for the nonlinear strain wave theory in a rod in Refs. 11, 13, and 14.

The restriction of the approach mentioned above is that the boundary conditions on a free lateral surface were not properly taken into account when these hypotheses were formulated. Direct substitution of these assumptions into the conditions of the absence of both normal and tangential stresses at the lateral surface does not result in zero stresses.

Generally speaking, the identity is not required because an asymptotic solution is assumed; however, the boundary condition failure indicates the possible neglect of several terms of the same order, which cannot be recovered from these hypotheses. As a result the changing of the functional form of a model nonlinear wave equation may appear or, at least, its coefficients may happen to vary. Therefore a refinement is required to the modeling of strain waves in a rod, with the boundary conditions on the lateral surface being taken into account.

A successful experimental generation of a strain soliton in a rod with varying cross section has not been mentioned up to now. Nevertheless, the strain soliton has been generated and observed in a uniform homogeneous nonlinearly elastic rod, using an experimental setup described in Refs. 15 and 16, and it revives interest in calculating and observing the strain soliton focusing in solids.

This paper will be organized as follows. A model will be

proposed in Sec. II to describe the propagation of a long nonlinear strain wave in an inhomogeneous rod. A procedure will be developed governing the analytical relations between displacements and strains in a rod, under which the complete *nonlinear* boundary conditions will be satisfied on the rod's free boundary with a given accuracy. It results in a nonlinear equation for the longitudinal strain waves, which will be compared with the theory recently developed in Refs. 17 and 11. An analytical solution will be found for an equation, describing the soliton amplitude variation due to the rod inhomogeneity. In Sec. III a method will be proposed for experimental observation of the solitary wave evolution in the inhomogeneous rod, based on the theory developed. The relationship will be derived, connecting the interference fringe shift and the amplitude of the longitudinal nonlinear strain wave. Finally the pioneering experimental results concerning the solitary wave focusing in a narrowing rod are discussed. It will be shown in Sec. IV that experimental data are in good agreement with the theory.

II. THEORY OF THE LONG NONLINEAR STRAIN WAVE PROPAGATION IN AN ELASTIC ROD WITH VARIABLE CROSS SECTION

A. Statement of the problem

Let us consider the wave propagation problem for an isotropic infinite nonlinearly elastic compressible rod. Introducing the cylindrical Langrangian coordinate system (x,r,φ), where x is the axis along the rod, $\varphi\epsilon[0,2\pi]$, $0\leqslant r\leqslant R(x)\leqslant R_0$, R_0 a constant, one can write the displacement vector $\vec{V}=(u,w,0)$, if torsions can be neglected. Basic equations, describing the nonlinear wave propagation in the initial configuration, are obtained from the Hamilton principle, requiring the variation of the action δS to be equal to zero:

$$\delta S=2\pi\delta\left(\int_{t_0}^{t_1}dt\left(\int_{-\infty}^{\infty}dz\int_0^R r\mathcal{L}dr\right)\right). \tag{1}$$

The internal integration in Eq. (1) is to be done for $t=t_0$, when the rod is supposed to be in the natural initial conditions. The Langrangian density per unit volume, $\mathcal{L}$, is obtained as the difference of the kinetic energy density K and the volume density of the internal energy Π at the adiabatic deformation, i.e., the potential energy:

$$\mathcal{L}=K-\Pi=\frac{\rho_0}{2}\left[\left(\frac{\partial u}{\partial t}\right)^2+\left(\frac{\partial w}{\partial t}\right)^2\right]-\Pi(I_k). \tag{2}$$

Here ρ_0 is the rod material density at $t=t_0$, while I_k, $k=1,2,3$ are invariants of the Cauchy-Green finite deformation tensor $\mathbf{C}$:

$$I_1(\mathbf{C})=\mathrm{tr}\mathbf{C},\quad I_2(\mathbf{C})=[(\mathrm{tr}\mathbf{C})^2-\mathrm{tr}\mathbf{C}^2]/2,\quad I_3(\mathbf{C})=\det\mathbf{C}. \tag{3}$$

The Murnaghan approximation of the deformation energy is chosen because it is valid for a wide class of nonlinearly elastic materials:[5]

$$\Pi=\frac{\lambda+2\mu}{2}I_1^2-2\mu I_2+\frac{l+2m}{3}I_1^3-2mI_1I_2+nI_3. \tag{4}$$

It is equivalent to a formal expansion of a scalar in a power series with respect to invariants of a second-rank tensor, obtained by Landau and Rumer.[18] The coefficients in Eq. (4) depend on the second-order elastic moduli, the Lame coefficients (λ,μ), as well as on the third-order elastic moduli, the Murnaghan moduli (l,m,n).

We will be aiming at the study of long nonlinear longitudinal strain waves (density waves), which will require some simplifications, namely, the relationships between longitudinal and transversal displacements u and w. To find them one needs to satisfy the boundary conditions on the free lateral rod surface $r=R(x)$, namely, the absence of both the normal and tangential stresses at every moment. We introduce the small parameter ε, taking into account that the waves under study should be *elastic* waves with sufficiently small magnitude B, $B\ll 1$, as well as sufficiently long waves with length L, so that the ratio $R_0/L\ll 1$, where R_0 is the maximal value of $r(x)$ along the rod. The most important case occurs when both nonlinear and dispersive features are *in balance* and *small enough:*

$$\varepsilon=B=\left(\frac{R_0}{L}\right)^2\ll 1. \tag{5}$$

We introduce $\tilde{U}\equiv BL$ as a scale for displacements u and w, and L as a scale for the coordinate along the rod axis, while R_0 is for the coordinate along the rod radius. Then the boundary conditions of the absence of stresses at the free lateral surface are obtained in dimensionless form by equating to zero the corresponding dimensionless components P_{rr} and P_{rx} of the Piola-Kirchhoff tensor $\mathbf{P}$,[5] that are written in power series of ε for convenience:

$$(\lambda+2\mu)w_r+\lambda\frac{w}{R}+\varepsilon\left[\lambda u_x+\frac{\lambda+2\mu+m}{2}u_r^2+\frac{3\lambda+6\mu+2l+4m}{2}w_r^2+\frac{(\lambda+2l)}{2}\left(\frac{2ww_r}{R}+\frac{w^2}{R^2}\right)\right]$$

$$+\varepsilon^2\left((\lambda+2l)u_xw_r+(2l-2m+n)\frac{wu_x}{R}+(\mu+m)u_rw_x\right)+\varepsilon^3\left(\frac{\lambda+2l}{2}u_x^2+\frac{\lambda+2\mu+m}{2}w_x^2\right)=0 \tag{6}$$

and

$$\mu u_r+\varepsilon\left(\mu w_x+(\lambda+2\mu+m)u_r w_r+(2\lambda+2m-n)u_r\frac{w}{R}\right)$$
$$+\varepsilon^2\left[(\lambda+2\mu+m)u_x u_r+\left(\frac{2m-n}{2}\right)\frac{w w_x}{R}+(\mu+m)w_x w_r\right]+\varepsilon^3(\mu+m)u_x w_x=0. \quad (7)$$

The unknown functions u and w will be expanded in a power series of ε:

$$u=u_0+\varepsilon u_1+\varepsilon^2 u_2+\cdots, \quad w=w_0+\varepsilon w_1+\varepsilon^2 w_2+\cdots. \quad (8)$$

Substituting Eqs. (8) into Eqs. (6) and (7), and equating to zero all terms of the same order of ε, one can prove that the plane cross section hypothesis is valid, however in leading order only:

$$u_0=U(x,t), \quad w_0=0. \quad (9)$$

Terms of order $O(\varepsilon)$ provide the relationship for w_1 that coincides with the Love hypothesis (and proves its validity now):

$$u_1=0, \quad w_1=-\frac{\lambda}{2(\lambda+\mu)}rU_x=-\nu r U_x \quad (10)$$

(ν is a Poisson coefficient), while the next terms lead to additional terms. Therefore for $i=2,3$ we find

$$u_2=\frac{\nu}{2}r^2U_{xx}, \quad w_2=0, \quad (11)$$

$$u_3=0,$$
$$w_3=-\frac{\nu^2}{2(3-2\nu)}r^3U_{xxx}-\left[\frac{\nu(1+\nu)}{2}+\frac{(1-2\nu)(1+\nu)}{E}\right.$$
$$\left.\times[l(1-2\nu)^2+2m(1+\nu)-n\nu]\right]rU_x^2, \quad (12)$$

where E is the Young modulus. Other terms from the series (8) for $i>3$ may be found in the same way; however, they will be omitted here because of no influence on the final model equation for the strain waves in the next section.

B. Longitudinal strain waves propagation in an inhomogeneous rod

The longitudinal strain waves equation can be derived using the Hamilton principle. In dimensional form it will contain small (but finite) additional terms to the linear wave operator, which describe the influence of both the nonlinearity and dispersion on the evolution of a *long elastic* wave. The problem may be solved in a dimensionless form also by means of an asymptotic solution in the power series on ε introduced in the previous section. However, for applications to physical experiments the dimensional form of the model equation is more convenient, while the Lagrangian (2) may be written without higher-order nonlinear and differential terms in the relationships for kinetic energy K and potential strain energy Π. Substituting expansions (8) into the formulas for K and Π, one can find, respectively,

$$K=\frac{\rho_0}{2}(U_t^2+\nu r^2[U_t U_{xxt}+\nu U_{xt}^2]), \quad (13)$$

$$\Pi=\frac{1}{2}\left(EU_x^2+\frac{\beta}{3}U_x^3+\nu E r^2 U_x U_{xxx}\right), \quad (14)$$

where $\beta=3E+2l(1-2\nu)^3+4m(1+\nu)^2(1-2\nu)+6n\nu^2$ becomes the only coefficient depending on the nonlinear elasticity of the rod. It is easy to see that the use of truncated expansions (8), containing only the three first terms, is sufficient to write relationships (13 and 14). Substituting them into Eq. (1) and calculating $\delta S=0$, one can obtain the following nonlinear equation:

$$U_{tt}-\frac{c_*^2}{R^2}\frac{\partial}{\partial x}[R^2U_x]$$
$$=\frac{1}{R^2}\frac{\partial}{\partial x}\left[\frac{\beta}{2\rho_0}R^2U_x^2-\frac{\nu}{4}\frac{\partial}{\partial x}(R^4U_{tt})+\frac{\nu^2}{2}R^4U_{xtt}\right]$$
$$+\frac{1}{R^2}\frac{\partial}{\partial x}\left[\frac{\nu c_*^2}{4}\left(R^4U_{xxx}+\frac{\partial^2}{\partial x^2}(R^4U_x)\right)\right]$$
$$-\frac{\nu R^2}{4}U_{xxtt}, \quad (15)$$

where c_* is the so-called ''rod'' wave velocity, $c_*^2=E/\rho_0$.

Therefore additional linear dispersive terms appear in the equation above due to the terms u_2 and w_3, resulting after the boundary condition fulfillment at the free lateral surface, and we obtained a *refined equation* in comparison with one obtained in Ref. 11.

Let us consider now the rod the cross section of which varies slowly along the x axis, which is described by a function $R=R(\gamma x)$, $\gamma\ll 1$. Introducing the notation $v=U_x$, $\tau=tc_*$ and differentiating Eq. (15) on x, we obtain an equation

$$v_{\tau\tau}-\frac{\partial}{\partial x}\frac{1}{R^2}\frac{\partial}{\partial x}\left(R^2v+\frac{\beta R^2}{2E}(v^2)+aR^4v_{\tau\tau}-bR^4v_{xx}\right.$$
$$\left.-4bR^3R_x v_x\right)=0, \quad (16)$$

deviating from those obtained in Ref. 11 with the dispersion term coefficients a and b, $a=-[\nu(1-\nu)]/2$, $b=-\nu/2$, which are different from the corresponding coefficients a

$=\nu^2/2$, $b=\nu^2/[2(1+\nu)]$ in Ref. 11 . Two first terms here describe a common linear wave, the third governs the nonlinearity, and the two following terms are responsible for the dispersive features of a waveguide, while the last term, being of the same order, looks like a dissipative one, but occurs due to the cross section variation.

The uniformly valid asymptotic analysis proposed in Ref. 11 for the fourth-order perturbed partial differential equation (PDE) can be used formally for solution to Eq. (16). To describe the evolution of a traveling strain wave v we introduce the phase variable θ and the slow variable $X\equiv\gamma x$, as follows:

$$\theta_\tau=-1, \quad \theta_x=A(X). \tag{17}$$

The solution to Eq. (16) will be found in new variables in the power series in γ:

$$v=v_0+\gamma v_1+\cdots. \tag{18}$$

Substituting Eq. (18) into Eq. (16) gives in leading order of γ the well-known solitary wave solution (''strain soliton'') for v_0,

$$v_0=\frac{3E}{\beta}\alpha\cosh^{-2}\{k(X)[\theta-\theta_0(X)]\}, \tag{19}$$

depending upon the varying parameter $\alpha=\alpha(X)$, $\alpha>0$, while A and k are expressed through it:

$$A^2=\frac{1}{1+\alpha}, \quad k^2=\frac{\alpha(1+\alpha)}{4R^2[a(1+\alpha)-b]}. \tag{20}$$

Both A and k will be real in Eq. (20) for most standard elastic materials (having the Poisson coefficient $\nu>0$) if the value of the function α is inside an interval:

$$0<\alpha<\frac{\nu}{1-\nu}. \tag{21}$$

Then the type of the strain wave (19) (compressive or tensile one) is defined only by the sign of the nonlinear coefficient β, which depends on the elasticity of the rod material, respectively.

Note that the use of the coefficient a, b values, defined previously in Ref. 11, results in another interval for α,

$$\alpha>0 \quad \text{or} \quad -1<\alpha<-\frac{\nu}{(1+\nu)}, \tag{22}$$

which prescribed the possibility of the existence both compressive and tensile waves for each sign of β.

Let us study a distortion of the solitary strain wave due to the ''geometrical'' inhomogeneity considered. The following differential equation for α arises from the secular term absence condition in order $O(\gamma)$:

$$\left(\ln\frac{R^2\alpha^2}{2kA^3}\right)_X+\frac{4bk^2R^2A^4}{5}(\ln 2R^4\alpha^2Ak)_X=0, \tag{23}$$

which after use of Eqs. (20) is reduced to a nonlinear first-order ordinary differential equation (ODE) for an amplitude variation,

$$\frac{R_X}{R}=\alpha_X\left(\frac{1}{6(1-D+\alpha)}-\frac{1}{2\alpha}-\frac{1}{3(1-D_1+\alpha)}-\frac{1}{3(1-D_2+\alpha)}\right), \tag{24}$$

where

$$D=\frac{b}{a}=\frac{1}{(1-\nu)}, \quad D_{1,2}=\frac{2\pm\sqrt{9-5\nu}}{5(1-\nu)}.$$

Taking the restrictions for α, Eq. (21), into account, we conclude that the expansion in the brackets on the right-hand side of Eq. (24) is always positive. Therefore the *magnitude* of the soliton will increase with the radius decrease. Direct integration of Eq. (24) yields

$$\frac{R^6\alpha^3[\nu+\alpha(2\nu-6/5)-\alpha^2(1-\nu)]^2}{(1-\nu)[\nu-\alpha(1-\nu)]}=\text{const}. \tag{25}$$

Routine analysis of the functions v_0, Eq. (19), and $v_{0,x}$ shows that the distortion of the wave shape takes place apart from the amplitude variation. When the bell-shaped soliton propagates along the narrowing rod, its front side becomes steeper while the back one becomes smoother. Vice versa, the front side of the solitary wave, moving along the expanding rod, becomes smoother, while the back one steeper. The equation for the determination of an extremum of a derivative $v_{0,x}$,

$$\gamma\frac{R_X}{R}+\{k(1-\gamma\theta_{0,X})+\gamma k_X[\theta-\theta_0(X)]\}\tanh\{k[\theta-\theta_0(X)]\}=0, \tag{26}$$

shows that for wave propagation along the narrowing rod ($R_X<0$) the extremum is achieved for $\theta-\theta_0(X)>0$, while in an extending rod ($R_X>0$) for an inverse sign. Then the soliton accelerates in a narrowing rod and decelerates in the expanding one in comparison with the same soliton moving along a uniform (homogeneous) rod.

The exact formulas (20) and (25) may be easily simplified to analyze the wave parameter variations. The range of the strain wave amplitude change has to be restricted by a physical condition of the strain's elasticity:

$$|\sqrt{1+2C_{xx}}-1|<e_0, \tag{27}$$

where e_0 is the yield point of a material, and for most of elastic materials its value lies in the interval $10^{-4}-10^{-3}$.[19] Therefore α will have to be small enough, and the following approximations follow from Eqs. (20) and (25):

$$A=1, \quad k^2=\frac{\alpha}{4R^2(a-b)}, \quad \frac{\alpha}{\alpha_0}=\left(\frac{R_0}{R}\right)^2. \tag{28}$$

The most important feature of the next order asymptotic solution is in the appearance of a plateau, propagating behind the soliton (19) with much less velocity. The difference in the values of a and b calculated in the framework of two theories results in a quantitative deviation in the plateau amplitude value. However, it is of order $O(\gamma)$; hence its change will be small also in comparison with the value obtained in

Ref. 17. This deviation seems unlikely to be detected by means of the equipment used in our experiments, and this part of solution is omitted here.

III. EXPERIMENTAL OBSERVATION

A. Experimental method

It is well known that optical methods are preferable to study the transparent optical phase inhomogeneities. They allow one not only to visualize inhomogeneity but also to determine its parameters, and on the other side, being contactless, they do not introduce any disturbances in an object under study; see Ref. 20. All optical methods record the changes of the refractive index in an object, when studying the optically transparent phase inhomogeneities. Shadowgraphy is more convenient to record a considerable refractive index gradient, for example, caused by strong shock wave propagation. It was shown theoretically in our case that a strain soliton is a propagating long density wave of small amplitude. Interferometry is the most appropriate for the study of such waves because it allows one to observe and measure with sufficient accuracy even small refractive index variations.

Holographic interferometry, used in our experiments, has several advantages in comparison with conventional optical interferometry. In particular, limitations on the optical quality are considerably lower because wave fronts to be compared pass through the same optical path. For this reason both waves are distorted *to the same extent* and possible defects in the optical elements and experimental cell do not affect the resulting interference pattern.

However, the choice of an optical recording method allows one to study, in general, only elastic materials, which are transparent for the given light wave length. The approach must be modified for an opaque material investigation.

Let us estimate the parameters of the initial pulse from which the strain soliton may be formed. Strain solitary waves cannot propagate with arbitrary velocity, and below we shall show the existence of an ''allowed'' velocity interval, beyond which the propagation of strain solitons is not possible (in contrast to our previous model,[11] where the ''dead zone'' of velocities was found, inside which the soliton cannot propagate). For a homogeneous (uniform) rod the solution (19) in the leading order problem for the longitudinal strain wave U_x has the form

$$U_x=\frac{3E\alpha}{\beta}\cosh^{-2}k_0(x\pm Vt), \tag{29}$$

while the soliton parameters depend on velocity as follows:

$$\alpha=\frac{V^2}{c_*^2}-1, \quad k_0^2=\frac{(V^2-c_*^2)V^2}{2\nu R^2c_*^2[c_*^2-(1-\nu)V^2]}. \tag{30}$$

One can see that the velocity V chosen to be positive should satisfy the inequalities at $1/2\geqslant\nu>0$,

$$1<\frac{V^2}{c_*^2}<\frac{1}{1-\nu}, \tag{31}$$

while at $-1<\nu<0$,

TABLE I. Type of solitary waves that are dependent on the nonlinearity coefficient β, the Poisson coefficient ν, and the velocity interval V^2/c_*^2.

Wave type	β	ν	V^2/c_*^2
Compression	<0	>0	$(1,\ 1/(1-\nu))$
Extension	>0	>0	$(1,\ 1/(1-\nu))$
Compression	>0	<0	$(1,\infty)$
Extension	>0	<0	$(0,\ 1/(1-\nu))$
Compression	<0	<0	$(1,\ \infty)$
Extension	<0	<0	$(0,\ 1/(1-\nu))$

$$\frac{V^2}{c_*^2}>1. \tag{32}$$

Obviously, for $\nu>0$ the existence of subsonic ($V<c_*$) compressive solitons is impossible for any elastic material parameter values, while supersonic solitons may propagate, having the velocity only from the interval (31) for most elastic materials. Therefore generation of compressive solitary strain waves requires an initial pulse generation [a shock wave, but a weak one to satisfy the limitation (27)] with the velocity from the interval (31). The ''allowed'' velocities for the generation of compressive (or tensile) soliton in materials with $\nu<0$ are shown in Table I.

To check that the excited strain wave possesses indeed the soliton feature to conserve its shape, it is necessary to follow in observations its propagation along an extended elastic waveguide. However, the more absorbing is a waveguide material for linear elastic waves; the much shorter distance is to be sufficient to detect the constant shape wave propagation.

Based on the results of the analysis presented above the transparent polystyrene SD-3 has been chosen as an appropriate material for waveguide manufacturing. The elastic properties of it are given by a set of parameters $\nu=0.35$, $\beta=-6\times10^{10}$ N/m^2, and $c_*=1.8\times10^3$ m/s; see Ref. 19. Polystyrene absorbs well both linear and shock elastic waves and it is widely used as an acoustic power absorber; see Refs. 21 and 22.

Shown in Fig. 1 is the optical scheme of the experimental setup used to generate and observe the strain solitons. The

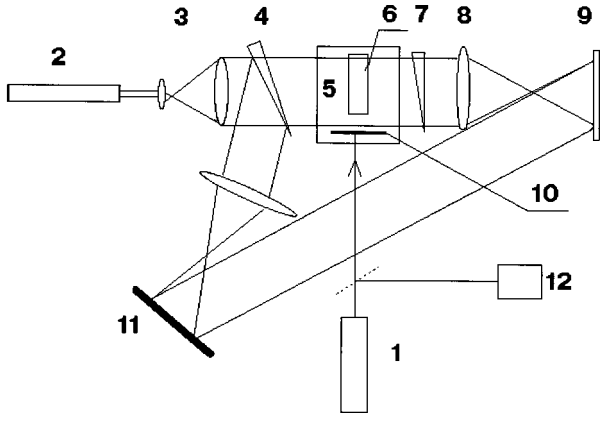

FIG. 1. Experimental setup for laser generation and optical observation of strain solitons.

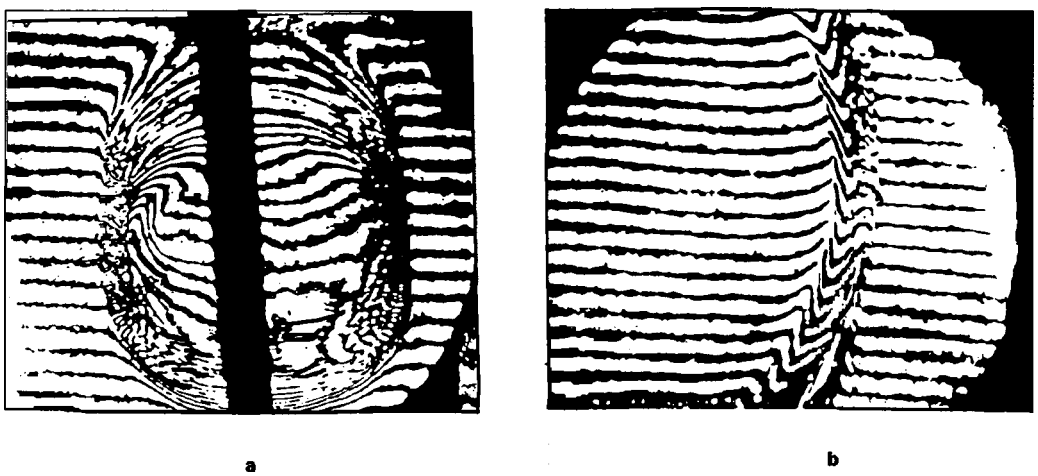

FIG. 2. Shock wave generation in water due to laser beam evaporation of metallic film target (a) and shock wave propagation near the rod (b).

apparatus consists of a device to produce the initial shock wave, a holographic interferometer for the recording of a wave pattern, a synchronizer, and a laser radiation energy meter.

In our experiments the strain soliton was formed from an initial shock wave, produced by action of the Q-switched ruby laser (1) (pulse duration is $15-20$ ns) on the metallic film target (10), placed in the water cell nearby the input edge of the rod (6). The laser pulse power density was measured by the energy meter (12) and was kept constant (equal to 2.3×10^{8} W/cm^2) during the experiment in order to avoid any inelastic strains in the material.

A second ruby laser (2) has been used for the hologram recording. The shutters of both lasers were synchronized by a multichannel generator of delayed pulses, which allowed us to record a wave pattern at a required time moment with the accuracy of order $1-2\times10^{-6}$ s. The light beam from the laser (2) (the beam diameter was 1.5 mm) was expanded by a telescopic system (3) up to a diameter equal to 50 mm, and then it was divided into the object and reference beams by a wedge (4). Passed through the wedge, the object beam was directed to the water cell (5) and to the rod (6) immersed in it. The central rod section was projected onto the hologram plane (9) by a lens (8), and the hologram of the focused image was recorded.

The first exposure of the hologram was carried out by the pulse from the laser (2) in the absence of a pulse from the laser (1), and so the hologram of undisturbed waveguide (6) was recorded. The second exposure was made by a laser pulse synchronized with the prescribed stage of the wave propagation. Observations were made in the transversal direction, and two cutoffs were made parallel to the rod axis in order to make transparent the central part of the rod. The carrier fringes on interferograms, obtained due to the reconstruction of doubly exposed holograms, occurred due to the wedge (7) turn between the exposures. The longitudinal strain wave patterns were recorded at various distances from the input edge of the rod, which was attained by the cell displacement along the axis of wave propagation.

Recently in Ref. 23 we have reported the study of a shock wave produced in water by the laser explosive evaporation of a metallic film target immersed in water. It was shown that such a shock wave (see Fig. 2) exhibits a very narrow compressive area (0.1–0.2 μm wide) followed by a considerable rarefaction area (1 mm wide) of small amplitude. The parameters of this shock wave satisfy the conditions required for strain soliton generation.[14] The proximity of wave impedance values for water and polystyrene allows us to enter the wave energy into the rod without considerable losses of power at the liquid/solid interface.

B. Experimental data processing

The soliton parameters were calculated based on the data of the holographic interferograms obtained. Note that the interferometric pattern does not exhibit a standard bell-shaped image of a shallow water soliton since the strain soliton is, in fact, a *longitudinal* density wave in a solid.

The soliton amplitude can be calculated using the interference fringe shift Δk measured in the interferogram. Let $2h$ be a distance passed by the recording light across the rod, i.e., precisely the distance between two longitudinal cutoffs. Before the deformation the phase variation $\Delta\phi_1$ of the light wave having length Λ is caused by the laser light propagation along the distance $q-2h$ through the water and the distance $2h$ through the rod (where q is the distance between the cell walls):

$$n_0(q-2h)+2hn_1=\frac{\Lambda}{2\pi}\Delta\phi_1. \tag{33}$$

Here n_0 and n_1 are the refraction indices of water and the elastic material before deformation, respectively. After the deformation the refraction index value of the rod changes to n_2. Moreover, the distances, which light passes through the rod and water, vary due to the deformation of the rod. As a result we obtain the formula for the magnitude of the light wave phase variation $\Delta\phi_2$:

$$n_0(q-2h-2\Delta h)+n_2(2h+2\Delta h)=\frac{\Lambda}{2\pi}\Delta\phi_2. \tag{34}$$

Evidently, the interference fringe shift Δk is defined as

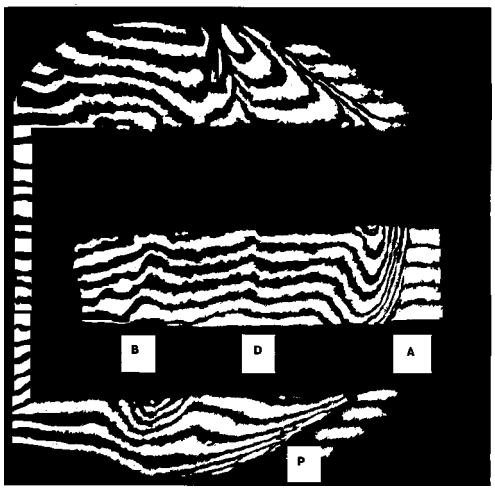

FIG. 3. Interferogram of the strain wave pattern near the input edge of the rod.

$$\Delta k = \frac{\Delta\phi_2 - \Delta\phi_1}{2\pi}. \tag{35}$$

The new value of the refraction index of the deformed rod, n_2, is caused by the local density variation:

$$\frac{\Delta\rho}{\rho} = \frac{n_2 - n_1}{n_1 - 1}, \tag{36}$$

which can be easily obtained following the Lorenz-Lorentz formula.[12] On the other side, one can obtain the density variation from the solution of a static linear problem on uniaxial compression (or tension) (see Ref. 5) and as a result the following relationship is valid:

$$\frac{\Delta\rho}{\rho} = U_x(2\nu - 1). \tag{37}$$

Then we get finally from Eq. (35)

$$U_x = -\frac{\Lambda\Delta k}{2h[(n_1-1)(1-2\nu)+\nu(n_1-n_0)]}. \tag{38}$$

The amplitude is determined by the maximal fringe shift value. Derivation of Eq. (38) shows that the length L of the solitary pulse may be directly determined from the interferogram as the length of the fringe perturbation between two undisturbed areas.

C. Observation of the soliton evolution in an inhomogeneous rod

The holographic wave pattern near the input edge of the rod is shown in Fig. 3. The left vertical black region represents an input section of the rod, and horizontal black areas above and below the central fringe area are cylindrical ''caps'' along the rod; see Fig. 4.

Black rectangular frames (as well as the gray frames in Figs. 5 and 6 below) surrounded the fringe pattern inside a rod appear due to the fact that the lateral surface of a rod beyond the central area of observation is not precisely perpendicular to the laser beam, i.e., not transparent, and therefore reflects the light.

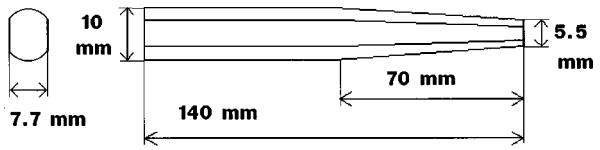

FIG. 4. Schematic of the rod with variable cross sections and cutoffs.

The wave pattern in Fig. 3 is complicated. On the interferogram one can see the shock wave (A), propagating along the rod, the remainder of the original shock wave (D), moving in a surrounding liquid and lagging behind the wave (A) due to the difference in velocities in solid and in water. The parts of wave (D) in water behind and ahead of the transparent rod appear due to observation in the direction transversal to the wave propagation. Moreover, a second shock wave (B) of a complex shape enters the rod also. This wave arises due to the partial refraction of the initial shock wave from the input edge and from the film target, respectively. The boundary conical waves (P) are observed also in a surrounding liquid, arising due to Poisson's expansion of the rod lateral surface when the compressive wave propagates inside it. The wave location detection (''which and where'') was done by means of velocity measurements of all of them using doubly exposed schlieren photography; see Ref. 20.

The choice of the rod's cross section variation is caused by two reasons. First, we were going to observe a geometrical inhomogeneity influence just on the strain soliton, and second, the experimental setup limitations should be taken into account. Measurements of the soliton amplitude in a homogeneous rod resulted in an estimation of the parameter $\varepsilon = O(10^{-3})$. When the inhomogeneity parameter γ is chosen to be $\gamma \ll \varepsilon$, then the possible variation of the initial rod radius ($R_0 = 5$ mm) at the distance 100 mm along the axis will be of order 0.1 mm or 2% from the initial value. The estimation of the amplitude change in this case by means of an approximation (28) shows that such a magnitude corresponds to the oscillations of the observed solitary wave front.[16] So it seems hardly possible to detect such a deviation using our experimental setup. Therefore the inhomogeneity parameter should be chosen as $\gamma \gg \varepsilon$.

It has to be noted, however, that a nonstationary process takes place in experiments in contrast to a quasistationary process governed by the asymptotic solution obtained above. When $\gamma \gg \varepsilon$ the inhomogeneity will change the initial pulse

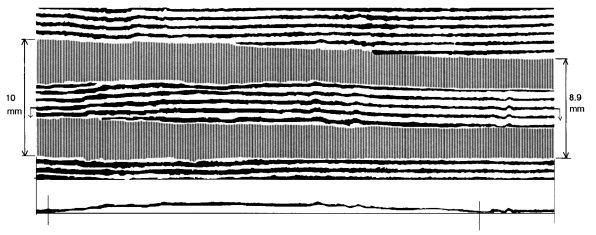

FIG. 5. Interferogram of the strain soliton in the nonlinearly elastic rod recorded at the end of the uniform cross section interval.

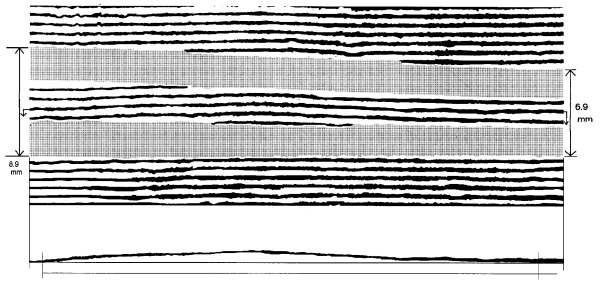

FIG. 6. Interferogram of the strain soliton recorded in the tapered nonlinearly elastic rod.

earlier than both nonlinearity and dispersion, and the strain soliton will hardly appear from an initial shock. Thus the rod cross section should remain constant at the distance required for soliton generation and separation, and begin to vary only after it. Experiments on the soliton generation in a homogeneous rod[15,16] showed that a soliton appears even at the distance of 60 mm (ca. $10R_0$) approximately from the input edge of the rod.

Based on this analysis, a rod 140 mm long was made of polystyrene with uniform and narrowing parts, as is shown in Fig. 4, and two cutoffs were made on the lateral surface for observation purposes. The rod radius decreases linearly from the value $R_0=5$ mm to the value $R=2.75$ mm along the distance 70 mm. In this case the inhomogeneity parameter $\gamma=0.032$ is much greater than the typical soliton amplitude $\approx 10^{-4}$ (Refs. 15 and 16) for the homogeneous rod.

Let us consider the holographic interferograms of the longitudinal strain soliton recorded in the transition interval from the rod with uniform cross section to its tapered part at the distance 40–90 mm from the edge of the rod (Fig. 5) and in the interval 75–125 mm (Fig. 6), where rod is tapered. The diameter of the recording beam is equal to 50 mm approximately. For convenient experimental data processing one of the disturbed interference fringes inside the rod (marked with arrows) was extracted from and placed below the interferogram. Fringes in the surrounding liquid remain undisturbed (horizontal), which confirms that the observed wave propagates inside the rod.

The shape of the strain wave was reconstructed by means of Eq. (38) using the following values of parameters: $n_0=1.33$, $n_1=1.6$, $\Lambda=7\times10^{-7}$ m, and $\nu=0.35$. It must be taken into account that light passes the different distances $2h$ in different cross sections. At the interval where the cross section remains uniform (Fig. 5), we have $2h=2h_0=7.75\times10^{-3}$ m, while the measured cross sections for the tapered rod's part are shown in Table II.

One can see that the maximal fringe shift on both interferograms is almost equal to the width between two neighboring fringes, i.e., to one fringe width. Substituting the data from Table II into Eq. (38), one can calculate finally the soliton parameters and obtain the soliton evolution in the tapered rod; see Fig. 7. The envelope lines are drawn there after interpolation. For convenience the compressive waves, having a negative amplitude, are shown in the first quadrant.

IV. DISCUSSION AND CONSLUSIONS

Thus, using the laser generator of weak shock waves and the holographic setup, we have made a generation, detection, and record of the strain solitary wave (the soliton) inside nonlinearly elastic both uniform and narrowing solid waveguides (the rods).

TABLE II. Light path distance measurements inside the deformed narrowing rod.

Distance from the input edge (mm)	Diameter of the rod (mm)	Light path distance $2h$ (mm)
50	10	7.75
65	10	7.75
70	10	7.75
75	9.8	7.45
80	9.5	7.2
85	9.2	7.0
90	8.9	6.8
95	8.6	6.6
100	8.3	6.3
105	8.0	6.1
110	7.7	5.8
115	7.5	5.7
120	7.1	5.4
125	6.9	5.0

The following arguments may confirm the observation of the genuine strain solitary wave in our experiments.

First, there is no tensile area behind the observed long compressive wave (having a length $\lambda>7R$), which is a typical feature of localized nonlinear waves. Tensile areas, if any, can be easily detected using the same apparatus: The fringes will be shifted in the opposite direction. However, deformation of the rod behind the soliton was studied in detail, and nothing was observed there except straight fringes; i.e., the rod was free of strain again after the soliton propagation.

Second, even at distances exceeding dozens of rod's radii, both the shape and the wave parameters remain permanent

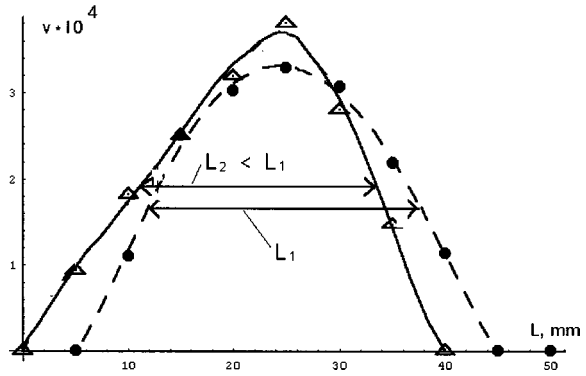

FIG. 7. Focusing (amplification) of longitudinal strain soliton. Two graphs of ''strain v vs solitary pulse width L'' are drawn after interpolation. Solid circles and the dashed interpolative line both correspond to experimental data measured on a 40–60 mm interval of the rod's length; open triangles and the solid interpolative line correspond to them on a 75 – 125 mm interval.

and do not exhibit any essential distortions in the uniform rod, as was shown recently;[16] that is, the nonlinear strain wave possesses one of the most distinctive features of a soliton. The distance chosen for our observations seems to be sufficiently large, because polystyrene is well known to be an effective absorber of acoustic and shock waves. The last was confirmed by considerable decay of the shock wave, which moved ahead of the soliton, as is shown in Figs. 5 and 6.

The enlargement of the amplitude scale allows us to visualize the main features of the solitary wave in the tapered rod; see Fig. 7. All the features predicted by our theory appear in experiments, namely, the increase of the amplitude, the steepness of the wave front, and smoothness of its back, i.e., asymmetric deformation of the bell-shaped soliton. Moreover, the characteristic width of the pulse shown in Fig. 6, $L_1=25.2$ mm, in the homogeneous part of the rod at the one-half amplitude level is visibly greater than a similar value, $L_2=22.3$ mm, in the narrowing part; hence the width of the localized strain solitary pulse decreases along the tapered rod.

Finally, simultaneously both an increase of the amplitude and a decrease of the width (i.e., the focusing) are distinctive for the nonlinear localized wave in a tapered waveguide, while the parameters of the linear strain wave are independent and defined by the initial or boundary conditions only.

The abilities of our experimental setup do not allow us to measure directly the soliton acceleration caused by the narrowing cross section along the rod.

However, all other details of the distortion of the wave observed (Fig. 7) compared with those theoretically predicted for the strain soliton, Eq. (19), lead to the conclusion that both the strain soliton and its focusing were observed, indeed, in our experiments. Fortunately we detected also both a steepening of the soliton front and a simultaneous smoothening of its back (Fig. 7) in close correspondence with a theoretical predicition of a soliton shape variation when focusing.

Therefore, the possibility was shown to transfer elastic energy at long distances without losses even in materials having a considerable absorbtion (dissipation) even for shocks. We proved in experiments that the elastic strain soliton is not absorbed even at distances much greater than the standard linear dissipation length for polystyrene. Presumably it means that the nonlinear absorbtion is much less than the linear one that does not affect the soliton; this problem requires further analysis.

The measurement of the wave amplitude is supposed to be quite plausible for comparison with the theory. One can see in Figs. 5 and 6 that the maximal amplitude of the strain soliton is achieved at the distances 60 and 95 mm from the rod input edge, respectively. Then from the estimation (38) we obtain soliton magnitudes equal to 3.29×10^{-4} in the interval 40–90 mm (Fig. 5) and to 3.83×10^{-4} for the interval 75–125 mm (Fig. 6). Therefore the soliton magnitude increases 1.16 times. The estimation using the simplified formulas (28) and a length dependence of the kind $R=R_0-\gamma(x-70)$ gives the amplification as 1.31 times, which is in good agreement with the experimental data.

However, some new theoretical results cannot be checked still in our experiments and require further study, namely, the following.

(i) In Sec. I A a refined theory was proposed to describe the nonlinear strain waves in a rod, improved by means of a precise fulfilment of the boundary conditions on a free lateral rod surface. The differences in the dispersive terms coefficients values in Eq. (16) result in a variation of the value of the soliton parameter k, Eqs. (20). The value of $1/k$ may be considered as the ''width'' of a soliton. Calculations based on the experimental data for a homogeneous rod show a 20–25% alteration in its value with respect to those found on the basis of a previous theory.[11,13] However, the concept of a soliton width is rather conventional; therefore this particular deviation between the two theories is rather difficult to confirm in our experiments.

(ii) The upper ''speed limit'' was found in Sec. II A for velocities (31) of a soliton in any elastic material, and the ''allowed zone'' for velocities was found to exist, outside of which neither generation nor propagation of a soliton are possible. The upper value of the limit (31) was not proved in our experiments because the soliton amplitude corresponding to this velocity provides an inelastic strain in polystyrene.

(iii) The observation of the amplitude dependence upon the Poisson coefficient ν is expected to be of interest for applications found by means of the exact formula (25).

The advantages of the theoretical description proposed here are of importance for the study of periodical, particularly, cnoidal waves, because the deviation in the values of k will correspond to the deviation in the wave lengths, which can be measured in experiments with reasonable accuracy. Another problem for which the refined theory should be applied is wave propagation along a waveguide embedded in an external medium. The theory also may be used for a soliton focusing study in 2D waveguides, in particular, in plates.

ACKNOWLEDGMENTS

The support of the Russian Federation Government and the International Science Foundation (Grant No. R56300) is gratefully acknowledged.

[1] Nature **376**, 373 (1995).

[2] M. Ablowitz and H. Segur, *Solitons and the Inverse Scattering Transform* (SIAM, Philadelphia, 1981).

[3] J.F. Bell, in *Encyclopaedia of Physics*, edited by S. Flügge (Springer, Berlin, 1973), Vol. YIa/1.

[4] D.R. Bland, *Nonlinear Dynamic Elasticity* (Blaisdell, Waltham, MA, 1969).

[5] A.I. Lurie, *Nonlinear Theory of Elasticity* (Elsevier, Amsterdam, 1990).

[6] P. Pleus and M. Sayir, J. Appl. Math Phys. (ZAMP) **34**, 192 (1983).

[7] H.D. McNiven and J.J. McCoy, in *R. Mindlin and Applied Mechanics*, edited by G. Herrmann (Pergamon, New York, 1974), pp. 197–226.

[8] R.T. Shield, Trans. ASME, J. Appl. Math. **50**, 1171 (1983).
[9] *Nonlinear Waves in Solids*, edited by A. Jeffrey and J. Engelbrecht (Springer, Wien, 1994).
[10] A.E.H. Love, *A Treatise on the Mathematical Theory of Elasticity* (Cambridge University Press, Cambridge, England, 1927).
[11] A.M. Samsonov, Sov. Phys. Dokl. **33**, 298 (1988).
[12] M. Born and E. Wolf, *Principles of Optics*, 2nd ed. (Pergamon Press, Oxford, 1964).
[13] A.M. Samsonov, in *Nonlinear and Turbulent Processes in Physics*, edited by R. Z. Sagdeev (Gordon and Breach, New York, 1984), Vol. 2, pp. 1029–1035.
[14] A.M. Samsonov and E.V. Sokurinskaya, Sov. Phys. Tech. Phys. **33**, 989 (1988).
[15] G.V. Dreiden *et al.*, Sov. Phys. Tech. Phys. **33**, 1237 (1988).
[16] G.V. Dreiden *et al.*, Tech. Phys. Lett. **21**, 415 (1995).
[17] A.M. Samsonov, Acta Techn. CSAV **42**, 93 (1997).
[18] L.D. Landau and Yu.B. Rumer, Phys. Z. Sowjetunion **11**, 18 (1937).
[19] I.N. Frantsevich, F.F. Voronov, and S.A. Bakuta, *Elastic Constants and Elastic Moduli for Metals and Non-metals* (Naukova Dumka, Kiev, 1982).
[20] G.V. Dreiden *et al.*, Thermophys Aeromech. **1**, 143 (1994).
[21] V.A. Shutilov, *Foundations of the Physics of Ultrasound* (Leningrad University Press, Leningrad, 1980).
[22] A.V. Bushman *et al.*, J. Exp. Theor. Phys. **82**, 895 (1996).
[23] M.A. Harith *et al.*, J. Appl. Phys. **66**, 5194 (1989).